Interplay of compressional and vortical nuclear currents in overtones of the isoscalar giant dipole resonance

Şerban Mişicu*,†
Physics Division, Argonne National Laboratory, Argonne, Illinois 60439, USA
(Received 30 August 2005; published 1 February 2006)

Within a semiclassical nuclear Fermi-fluid dynamic approach, the properties of the isoscalar giant dipole resonance (ISGDR) and the structure of various electromagnetic characteristics associated with the most important states building this resonance are investigated. The apparent puzzling outcome of microscopic predictions that the ISGDR distribution is split into two main broad structures is confirmed within the presented macroscopic approach by the occurrence of a "low-lying" and a "high-lying" state, as the first two overtones of the same resonance. Macroscopicaly, they are pictured as a combination of compressional and vortical nuclear flows. The second part of the paper analyzes the electromagnetic structure of the ISGDR relevant to reactions with inelastically scattered electrons and the relation between the vorticity and the toroidal dipole moment. The relative strengths of the compressional and vortical collective currents are evaluated by means of electron-scattering sum rules.

DOI: 10.1103/PhysRevC.73.024301 PACS number(s): 24.30.Cz, 21.10.Ky, 13.40.Gp, 25.30.Dh

I. INTRODUCTION

Recently, the College Station group [1] reported experimental results on the isoscalar $E1$ strengths in three proton magical nuclei (^{90}Zr, ^{116}Sn, and ^{208}Pb) using inelastic scattering of 240 MeV α particles at small angles. The authors concluded that the isoscalar $E1$ strength distribution in each nucleus is shared mainly between two components, one located at low energy and another at higher energy. In a subsequent publication, this group presented new data on the isoscalar giant dipole resonance (ISGDR) [2]. For ^{116}Sn, ^{144}Sm, and ^{208}Pb, the low-energy peak falls in the interval $(1.71\text{–}1.92)\,\hbar\omega$, whereas the high-energy peak lies between 3 and $3.2\,\hbar\omega$. The upper component covers approximately three times more of the energy-weighted sum rule compared to the lower component. Similar values for the two peaks for ^{208}Pb are given in [3]: 1.80 and $3.25\,\hbar\omega$. Previously, Morsch *et al.* [4] found for the high-lying component in ^{208}Pb a centroid of 21.3 ± 0.8 MeV, which corresponds to $(3.15 \pm 0.12)\,\hbar\omega$. Therefore, experimentally, the lower-energy component has a value very close to the isovector giant dipole resonance (IVGDR) centroid which is $\approx 2\hbar\omega$, whereas the higher-energy component is located in the same region as the electric octupole resonance, i.e., $\approx 3\hbar\omega$.

On the theoretical side, numerous studies have aimed at disclosing the features of these exotic modes. The usually accepted macroscopic picture of the ISGDR is a "hydrodynamic density oscillation" in which the volume of the nucleus remains constant and the proton-neutron fluid oscillates in phase back and forth through the nucleus in the form of a compression mode [5,6]. Microscopic calculations using strengths associated with the nonisotropic compression, namely, the "dipole squeezing" operator $D = \sum_i r_i^3 Y_{1\mu}(\hat{r}_i)$, are stressing the importance of the high-lying ISGDR ($\approx 3\hbar\omega$) [7–9]. They also predict a rather fragmented peak at smaller energies ($\approx 2\hbar\omega$) [10–13]. A similar, bimodal structure was obtained within the fully consistent relativistic Hartree-Fock plus random-phase-approximation (RPA) framework [14].

The first macroscopic models of electric resonances were primarily concerned with describing the ISGDR as density fluctuations of a nuclear liquid drop. In an apparently overlooked paper, available only in German [15] and published a couple of years after the emergence of the incompressible fluid model of the IVGDR, the isoscalar dipole eigenfrequencies of a spherical nucleus were determined for the first time. The investigations of the College Station Kyiw group [16] pointed out that considering only compressional components in the velocity field and neglecting the relaxation effects within the nuclear-fluid dynamics leads to an overestimation of the energies of the 1^- resonances with respect to the experimental values.

Other macroscopic approaches have aimed at describing the giant resonances (including the 1^-, $T = 0$ state) by allowing for vortical components along with or without the longitudinal compressional or divergenceless velocity field. Deriving conservation equations, such as the continuity equation, and equations of motion such as the Navier-Stokes or Lamé revealed that the macroscopic velocity field admits also shear (transverse) components [17]. In Ref. [18], after making some simplifications to the work in [17], which we are going to dismiss in the present study, an isoscalar 1^- state of pure vortical character was derived. Subtracting the center-of-mass motion, the associated velocity field reads

$$\boldsymbol{v}_\mu{}^{\text{tor}}(r,\theta,\phi) = \nabla \times \nabla \times \boldsymbol{r}\left(r^3 - \tfrac{5}{3} r \langle r^2\rangle\right) Y_{1\mu}(\theta,\phi). \quad (1)$$

Most important is that this study for the first time made a connection to the toroidal class of electromagnetic multipole moments introduced earlier by Dubovik and Cheshkov [19]. The theoretical search for a vortexlike isoscalar dipole electric excitation associated with the toroidal dipole moment (dipole torus mode) was continued in the nuclear-fluid dynamics frame [20,21]. Reference [21] substantiated the elastic character of

*On leave from: Department for Theoretical Physics, National Institute for Nuclear Physics, P.O. Box MG6, Bucharest, Romania.
†Electronic address: misicu@theor1.theory.nipne.ro; URL: http://www.theory.nipne.ro/misicu/

this mode, since a nucleus without shearing properties cannot withstand transverselike oscillations, and evaluated for the first time the (e, e') form factors corresponding to the excitation of this isoscalar 1^- resonance. The radial part of the transverse electric form factor corresponding to the electroexcitation of the dipole torus mode was found to vary as $j_3(qr)/qr$.

Apart from the quest of the toroidal nature of the ISGDR, there are also other issues related to the enhancement of these electromagnetic transitions for other types of collective electric excitations. The electric dipole spin waves were identified in [22] to have a nonvanishing magnetization-dependent part of the toroidal dipole operator. In [23] and [24], the fingerprints of the dipole toroidal moments in the electromagnetic properties of nuclear rotational states were examined for the first time in the literature. In [24], it was inferred that the strong deviations from predictions of adiabatic theory for the absolute values of $E1$ transitions in the Coulomb excitation of ^{226}Ra are related to the enhancement of toroidal transitions between the ground state and the lowest negative parity band.

The revival of interest in the role played by toroidal moments in the excitation of the isoscalar dipole resonance was caused by a recent publication [25] that aimed to evaluate the $E1$ strength distribution in spherical nuclei where the relativistic mean-field (RMF) formalism + RPA calculations were previously unable to provide a satisfactory agreement with the experimental data on the positions of the ISGDR resonances. Using the toroidal dipole operator corrected for c.m. motion instead of the squeezing operator, broad resonant peaks were assigned in the low- ($\leqslant 2\hbar\omega$) and high-energy ($>3\hbar\omega$) regions of the strength distribution for ^{208}Pb.

Commenting on the results reported in [25], the short note [26] stressed the fact that the low-lying vortical mode, as inferred from macroscopic calculations [18,20,21], is different from the so-called pigmy resonance which is in the vicinity of $1\hbar\omega$, and that the centroids provided by the nuclear-fluid approaches [20,21] are still providing a qualitatively good agreement with the (α, α') scattering data. In this respect, the merit of [25] is that it offers for the first time in the literature a microscopic calculation of the toroidal content of ISGDR states and confirms the connection already established by macroscopic models between this electromagnetic characteristic and vorticity. Moreover, and this will be an important point in our present work, although not explicitly stated in the body of Ref. [25] but rather inferred from its Fig. 2, it indicated that for the high-lying states there is also a more or less important value of the toroidal strength, which implies that these excitations are not purely compressional but may also contain significant vortical admixtures.

The nature of collective flows in a range of excitation energy below 20 MeV for ^{208}Pb was more closely approached in [27], where calculations within the quasiparticle phonon model pointed to strong vorticity below $2\hbar\omega$ for the entire electric dipole response not only the isoscalar one.

II. NUCLEAR-FLUID DYNAMIC APPROACH

A macroscopic approach that goes partially along the lines already developed in a previous publication [21] is adopted. However, strong amendments are performed by including

(i) Full k content in the radial part of the collective field, and
(ii) A compressional elastic constant different from the shear elastic constant ($\lambda_{\mathrm{Lame}} \neq \mu_{\mathrm{Lame}}$) that draws it nearer to other Fermi-fluid dynamic approaches [16,17,28].

The procedure consists of taking moments of the Boltzmann equation, i.e., to integrate it in the momentum space with weights 1, p_i, $p_i p_j$, etc. The first two moments provide the continuity and the Navier-Stokes equation because their forms are similar to the well-known equations from hydrodynamics,

$$\frac{\partial \rho(\boldsymbol{r}, t)}{\partial t} + \nabla \cdot (\rho(\boldsymbol{r}, t)\dot{\boldsymbol{u}}) = 0, \tag{2}$$

$$\frac{\partial}{\partial t}(\rho(\boldsymbol{r}, t)u_i) + \sum_{j=1}^{3} \frac{\partial P_{ij}}{\partial x_j} = 0, \tag{3}$$

where ρ is the mass density, which is supposed to be of the sharp-edge type in the present work, $\boldsymbol{u}$ is the collective field (which vanishes in the ground state), whereas P_{ij} are stress tensor components. To these equations, the linearization procedure is applied such that

$$\rho(\boldsymbol{r}, t) = \rho_0 + \delta\rho(\boldsymbol{r}, t), \quad \boldsymbol{u} = \delta\dot{\boldsymbol{s}}, \quad P_{ij} = p\delta_{ij} + \delta\sigma_{ij}. \tag{4}$$

In the second equation of (4), the displacement field $\delta\boldsymbol{s}$ is introduced. The stress tensor is split into a diagonal part (normal pressure)

$$p = -\frac{1}{9m} K \rho_0 \dot{\mathcal{D}} \tag{5}$$

and a nondiagonal one (related to the shear)

$$\delta\sigma_{ij} = -\frac{4}{5m}\rho_0 \epsilon_F \left(\varepsilon_{ij} - \frac{1}{3}\delta_{ij}\mathcal{D}\right), \tag{6}$$

where K is the incompressibility coefficient of nuclear matter and ϵ_F is the Fermi energy. The scalar function

$$\mathcal{D} \equiv \nabla \cdot \delta\boldsymbol{s}$$

describes the compressibility of the displacement field $\delta\boldsymbol{s}$, and ε_{ij} are the components of the dyadic strain tensor [29]

$$\hat{\boldsymbol{\varepsilon}} = \tfrac{1}{2}\left(\nabla\boldsymbol{s} + \boldsymbol{s}\nabla\right).$$

After linearizing the equations of motion, we get

$$\begin{aligned} \delta\dot{\rho} &= \rho_0 \dot{\mathcal{D}}, \\ \rho_0 \delta\ddot{\boldsymbol{s}} &= (\lambda_{\mathrm{Lame}} + 2\mu_{\mathrm{Lame}})\nabla(\nabla\mathcal{D}) - 2\mu_{\mathrm{Lame}}\nabla \times \boldsymbol{\omega}, \end{aligned} \tag{7}$$

where, as in hydrodynamics ([29], p. 115), $\boldsymbol{\omega}$ denotes the vorticity vector which is proportional to the curl of the displacement field

$$\boldsymbol{\omega} \equiv \tfrac{1}{2}\nabla \times \delta\boldsymbol{s}.$$

The equation of motion (7) is identical to the Lamé equation ([29], pp. 60 and 94) known from the mechanics of deformable continua, where the Lamé elastic coefficients are provided by the properties of the nuclear Fermi fluid [16,28]

$$\lambda_{\mathrm{Lame}} = \frac{n_0 K}{9} - \frac{4}{15}n_0\epsilon_F, \quad \mu_{\mathrm{Lame}} = \frac{2}{5}n_0\epsilon_F.$$

For the incompressibility coefficient K, we use the fact that the excitation energy of the isoscalar giant monopole resonance (ISGMR), which is an isotropic volume oscillation, can be related to the compressibility of nuclei [30], i.e.,

$$E_{\mathrm{ISGMR}} = \left(\frac{\hbar^2 K}{m\langle r^2\rangle_0}\right)^{1/2} \approx 82A^{-1/3}.$$

The incompressibility coefficient and Lamé constants are numerically determined by using $r_0 = 1.12$ fm, $n_0 = 3A/4\pi R_0^3$, $k_F = 1.36$ fm, and $\epsilon_F = \hbar^2 k_F^2/2m$.

In what follows, a fundamental theorem of vector analysis is used ([29], p. 131) which states that every continuous vector field $\boldsymbol{V}$, which together with its derivative falls to 0 at large distances, can be decomposed into a divergenceless part $\boldsymbol{V}_\perp(\nabla\cdot\boldsymbol{V}_\perp = 0)$ and a curlless part $\boldsymbol{V}_{||}(\nabla\times\boldsymbol{V}_{||} = 0)$.

Then Eq. (7) separates into an equation for compressibility $\mathcal{D}$ and another one for vorticity $\boldsymbol{\omega}$, which describes the degree of shear of the displacement field for the case of an elastic body,

$$\ddot{\mathcal{D}} = c_L^2\Delta\mathcal{D}, \quad \ddot{\boldsymbol{\omega}} = c_T^2\Delta\boldsymbol{\omega}, \tag{8}$$

where $c_L = \sqrt{\lambda_{\mathrm{Lame}} + 2\mu_{\mathrm{Lame}}/\rho_0}$ and $c_T = \sqrt{\mu_{\mathrm{Lame}}/\rho_0}$ are the propagation velocities of the longitudinal (compressional) and transverse (shear) elastic waves in nuclear matter [28].

Assuming a harmonic variation in time with the fluctuating parts of the density and the displacement field, i.e.,

$$\delta\rho(\boldsymbol{r},t) = \rho(\boldsymbol{r})e^{i\Omega t}, \quad \delta\boldsymbol{s}(\boldsymbol{r},t) = \delta\boldsymbol{s}(\boldsymbol{r})e^{i\Omega t},$$

the compressibility and the vorticity are found to satisfy the scalar and vector Helmholtz equations, respectively,

$$\left(\Delta + \begin{Bmatrix} k_L^2 \\ k_T^2 \end{Bmatrix}\right)\begin{Bmatrix} \mathcal{D} \\ \boldsymbol{\omega} \end{Bmatrix} = 0, \tag{9}$$

corresponding to the wave numbers $k_{L,T} = \Omega/c_{L,T}$. In seismology the compressional wave is called the P wave, and the transverse wave, the S wave [31]. The S in its turn has two components: the *SH* wave (known as the poloidal in hydrodynamics or transverse electric in electrodynamics) and the *SV* wave (torsional or magnetic). For a nucleus with a sharp edge, one adopts a spherical geometry and the radial part is given by spherical Bessel functions, whereas the angular part can be written in terms of spherical harmonic vectors. Details can be found in the Appendix or in the literature [32]. Next we disregard the torsional component which is related to magnetic excitations [33] and consider only axial-symmetric displacement fields ($\mu = 0$). We then have for the longitudinal and poloidal components of the displacement field the expressions (A5) and (A7) derived in the Appendix. These expressions have to be further corrected in order to account for the center-of-mass motion. As in a preceding paper [21], the translational invariance of the collective velocity field results from the condition that the center-of-mass $\boldsymbol{R}_{\mathrm{c.m.}}$ is at rest

$$\delta\boldsymbol{R}_{\mathrm{c.m.}} = \frac{\int d\boldsymbol{r}\rho(\boldsymbol{r},t)\delta\boldsymbol{s}}{\int d\boldsymbol{r}\rho(\boldsymbol{r},t)} = 0. \tag{10}$$

Thus in the dipole case ($\lambda = 1$), the longitudinal and transverse displacement fields are

$$\begin{aligned}\delta\boldsymbol{s}_L(\boldsymbol{r},t) = \frac{1}{\sqrt{3}}a\bigg[&\left(j_0(k_L r) - \frac{3}{k_L R_0}j_1(k_L R_0)\right)\boldsymbol{Y}_{10}^0(\theta,\phi)\\ &+ \sqrt{2}j_2(k_L r)\boldsymbol{Y}_{12}^0(\theta,\phi)\bigg],\end{aligned} \tag{11}$$

$$\begin{aligned}\delta\boldsymbol{s}_T(\boldsymbol{r},t) = -\frac{1}{\sqrt{3}}b\bigg[&\sqrt{2}\left(j_0(k_T r) - \frac{3}{k_T R_0}j_1(k_T R_0)\right)\\ &\times \boldsymbol{Y}_{10}^0(\theta,\phi) - j_2(k_T r)\boldsymbol{Y}_{12}^0(\theta,\phi)\bigg].\end{aligned} \tag{12}$$

The corresponding corrected expression for the density fluctuation is produced by applying the continuity equation in (10) followed by the substitution of the longitudinal diplacement field (11). The integral relation between the corrected expression of the density fluctuation and the longitudinal displacement field reads

$$\int d\boldsymbol{r}\,\boldsymbol{r}\delta\rho = \rho_0\int d\boldsymbol{r}\nabla\times(\delta\boldsymbol{s}_L\times\boldsymbol{r}). \tag{13}$$

Eventually, we obtain for the density fluctuation an expression identical to the one derived in [16],

$$\begin{aligned}\delta\rho = a\rho_0\bigg(&j_1(k_L r)\Theta(R_0 - r)\\ &- \frac{1}{k_L}j_2(k_L R_0)\delta(R_0 - r)\bigg)Y_{10}(\theta,\phi).\end{aligned} \tag{14}$$

In order to derive the longitudinal and transverse wave numbers k_L and k_T and the constants a and b multiplying the displacements fields, boundary conditions for the force acting on the free surface of the nucleus have to be imposed. This force is obtained by projecting the dyadic stress tensor on the normal unit vector to the surface,

$$\boldsymbol{F} = \widehat{\boldsymbol{P}}\cdot\boldsymbol{e}_r. \tag{15}$$

Usually two types of boundary conditions are employed depending on what assumption has been made for the surface. Two kinds of bounding nuclear surfaces are distinguished for sharp-edge distributions: *rigid surfaces* on which no slip occurs (used in the liquid drop model to determine the "surfon" eigenvalues or in the hydrodynamic model of giant resonances [34] to determine the "gion" eigenvalues) and *free surfaces* on which no tangential stresses act. If we were to assume a rigid surface, then we would end up with a density fluctuation, and thus also with a velocity field containing admixtures of the c.m. motion. Actually, the expression of the fluctuation density (14), corrected for the c.m. motion, is compatible with the assumption of a free surface. The boundary conditions of a free surface require that the force fulfill the following two conditions [28,35]:

$$\begin{aligned}\boldsymbol{e}_r\cdot\boldsymbol{F}|_{r=R_0} &= P_{rr}|_{r=R_0} = 0,\\ \boldsymbol{e}_r\times\boldsymbol{F}|_{r=R_0} &= (\boldsymbol{e}_\phi P_{r\theta} - \boldsymbol{e}_\theta P_{r\phi})\big|_{r=R_0} = 0.\end{aligned} \tag{16}$$

These equations provide an infinity of eigenvibrations, but for the study of giant resonances only the first few are relevant. The boundary condition (16) allows also the determination

TABLE I. First four overtones provided by the eigenvalues of the boundary condition (16) and the vorticity/compressibility ratio for ^{208}Pb.

Overtone(n)	$k_L^{(n)}$ (fm^{-1})	$k_L^{(n)} R_0$	$\hbar\Omega_n$ (MeV)	$\hbar\Omega_n/\hbar\omega_0$	$r_n \equiv b_n/a_n$
1	2.05	3.05	11.56	1.67	1.94
2	3.93	5.86	22.19	3.21	−1.19
3	5.05	7.53	28.53	4.12	6.09
4	7.09	10.57	40.03	5.78	−4.03

of the ratio b_n/a_n which gives the admixture between the compressional (longitudinal) and vortical (transverse) field in a given state n,

$$r_n \equiv \frac{b_n}{a_n} = - \left. \frac{P_{rr}^{\mathrm{Longitudinal}}}{P_{rr}^{\mathrm{Transverse}}} \right|_{r=R_0} .$$

In Table I we list the first four roots (overtones) of the boundary condition plus the ratio of the transverse-to-longitudinal weights.

As already mentioned in the Introduction, the College Station and Osaka data confirm the existence of low- and high-energy components of ISGDR. For ^{208}Pb, the College Station group provided first 12.2 ± 0.6 MeV [1] and later [2], extending the continuum, 13.26 ± 0.3 MeV for the low-lying resonance, whereas for the high-lying resonance the values 19.9 ± 0.8 and 22.2 ± 0.3 MeV were reported. The Osaka group reported centroids lying at 12.5 ± 0.3 and 22.5 ± 0.3 MeV [3]. Obviously, the second overtone predicted in the nuclear Fermi-fluid formalism is in very good agreement with the latest data from College Station and Osaka. The first overtone is closer instead to the previously reported low-energy peak, the obvious tendency being an under evaluation of up to 15% of the latest experimental values. There could be several reasons why the low-lying peak is not predicted as well as the high-lying one. A possibility could be the drastic approximation of a sharp nuclear surface that can affect more of a toroidal vortex oscillation, such as the first overtone, that exhibits distortions of the displacement field over the entire nuclear surface, rather than a compressional oscillation which mostly affects nuclear matter at the north and south poles of the dipole motion. This conjecture could be inferred from Fig. 1, which displays the nuclear matter flow for the ISGDR overtones. However, the general bimodal trend of the ISGDR observed in experiment is reproduced by the fluid-dynamic formalism, as we shall see also in Sec. III for other nuclei.

One might also ask if for the third overtone, predicted at 28.53 MeV (Table I), there is any indication in the experiment. According to the most recent data (see Fig. 6 of [2]), for ^{208}Pb the uncertainties above 25 MeV are so large that it is difficult to draw any conclusion. Despite this, the authors of [2] do not exclude unobserved $E1$ strength at higher energy.

It is worthwhile to compare the results of this section with other theoretical works. The first three eigenfrequencies for the dipole density fluctuations as derived in the pioneering work of Woeste [15] have values very close to those of the density-vorticity waves listed in Table I: 1.78, 3.02, and 4.22$\hbar\omega$ compared to 1.67, 3.21, and 4.12$\hbar\omega$. Also, the estimation for the $T = 0$, $L = 1^-$ vortex mode from [18] (1.7$\hbar\omega$) is very close to the value derived in the present paper. In a previous paper dedicated to ISGDR [21], we constrained the collective velocity field to admit purely vortical flows and we considered the low-lying response of the Fermi liquid; whereas in the present approach, the full momentum content is taken into account. Therefore, although compressional components are occurring, the first overtone has a rather vortical character as can be easily inferred from the upper left panel of Fig. 1, and it displays the typical Hill-vortex pattern as already mentioned in [18,20,21]: nuclear matter flows around a vortex ring situated in the equatorial plane of the nucleus. Other works, based like [15] on the compressible and irrotational nuclear liquid drop, e.g. [36], fail to observe the first overtone. In such approaches, the necessity to correct the density fluctuation for the c.m. motion was not anticipated. For the second overtone, the compressional and vortical flows have almost an equal importance, which contradicts the entrenched picture of a compressional mode around 3$\hbar\omega$. However, there is to date no direct experimental indication of such a macroscopic property of this higher-lying isoscalar dipole resonance, and therefore the result that we report on this mode should not be excluded from debate. To a certain extent, the flow pattern of this mode (see upper right panel of Fig. 1) presents typical characteristics of a compressional mode: the concentration of nuclear matter flow inside the southern hemisphere and its depletion inside the northern hemisphere; at the same time, an opposite behavior of the density fluctuation is manifested at the north and south poles. For the third and fourth overtones (see lower left and right panels of Fig. 1), the flow is predominantly vortical. Although difficult to disclose from the flow patterns, the vortex structure becomes more intricate in the sense that instead of one vortex ring as was the case for the first overtone, we are dealing with two rings ($n = 3$ overtone) and three rings ($n = 4$ overtone) of lower intensity. Note that two successive rings have opposite rotational flows.

A quantitative way to assess the role of compressional and vortical flows is to introduce, following [35], the orientation averaged values of the collective velocity field divergence

$$\langle \mathcal{D} \rangle \equiv \left(\int \mathcal{D}^2 d\Omega \right)^{\frac{1}{2}}$$

and vorticity

$$\langle \boldsymbol{\omega} \rangle \equiv \left(\int \boldsymbol{\omega}^2 d\Omega \right)^{\frac{1}{2}} .$$

These two quantities are displayed in Fig. 2. In order to avoid the awkward effect on these two radial functions near the surface, which is caused by the sharp-edge distribution (see Ref. [35]), the curves drawn in Fig. 2 were computed by assuming a diffuse density distribution. Consequently, an additional peak in both $\langle \mathcal{D} \rangle$ and $\langle \boldsymbol{\omega} \rangle$ occurs in the surface region. Concerning vorticity, we remark for the first overtone that it attains a maximum at approximately $R_0/\sqrt{2}$, which corresponds to the critical points of the Hill vortex, a fact already pointed out in [21]. Inside the nucleus, compressibility increases almost linearly with the radius and is less important

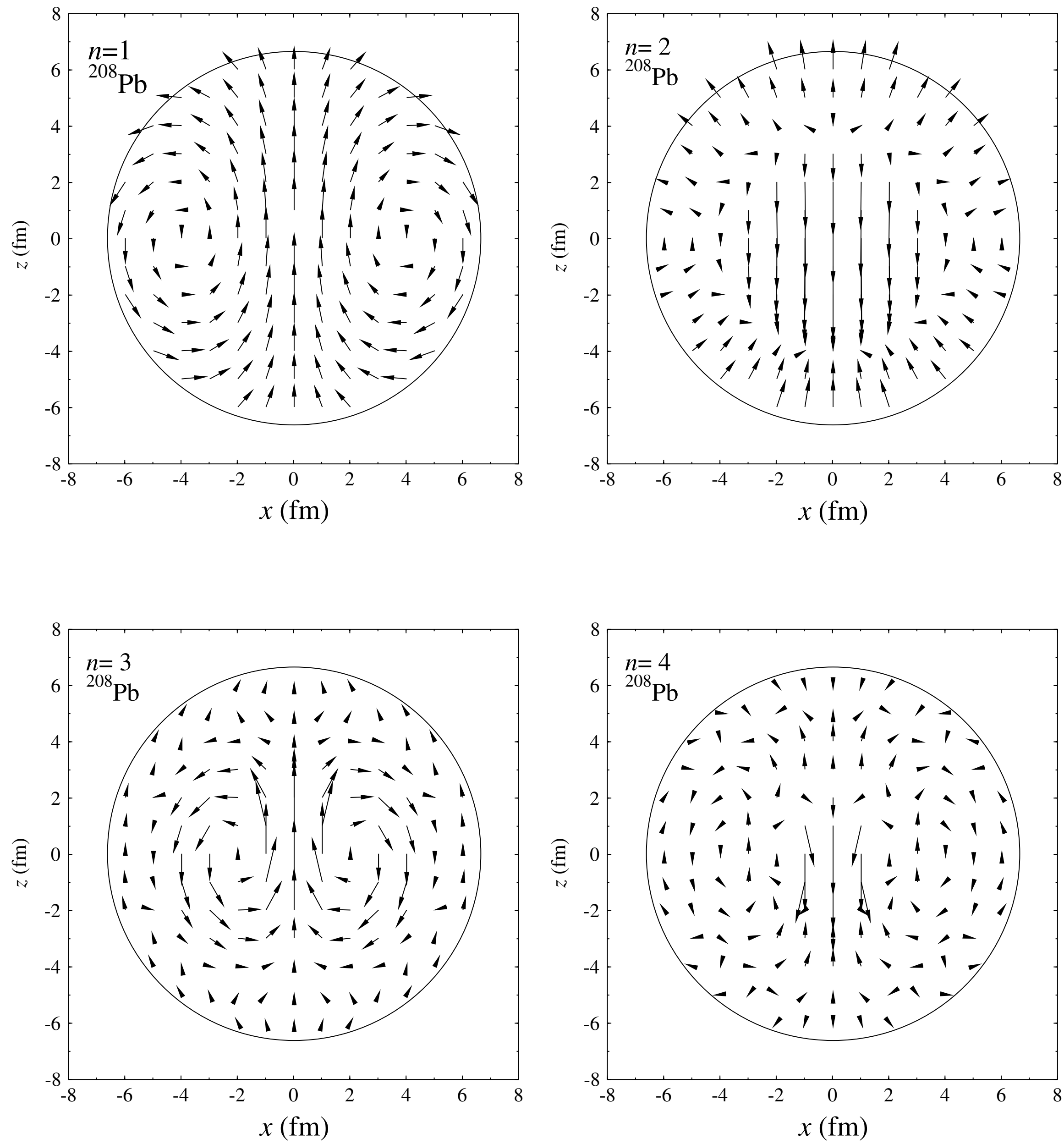

FIG. 1. Flow lines corresponding to the first four overtones of the ISGDR in ^{208}Pb.

than vorticity, thus confirming the previous assignment of this collective state to the dipole torus mode [18,20,21]. When the overtone number increases, the vortex with the largest strength migrates toward the center of the nucleus, and new ringlike vortices occur at larger radii. For overtones with $n \geqslant 2$, the compressibility develops maxima inside the nuclear sphere and plays a dominant role only for the $n = 2$ overtone (the $3\hbar\omega$ "compression mode") in the vicinity of the nuclear surface. The mixed (compressional+vortical) character of the $n = 2$ state can be also inferred from the self-consistent RPA calculations with Skyrme-type interaction performed in an old study [37] as well as in the relativistic mean-field approach from [14].

The procedure to quantize a continuum system, described by the equation of continuity and the equation of motion (7), is to expand $\delta\rho$ and $\delta \boldsymbol{s}$ in normal coordinates [38]:

$$\delta\rho(\boldsymbol{r}, t) = \sum_n \rho_n(\boldsymbol{r})\alpha_n(t), \quad \delta \boldsymbol{s}(\boldsymbol{r}, t) = \sum_n \boldsymbol{s}_n(\boldsymbol{r})\alpha_n(t). \quad (17)$$

These sums are running after the values of $k_L(k_T)$ allowed by the boundary condition (16), i.e., after the overtones n. For the expression of kinetic energy in the newly introduced collective coordinates α_n, we have

$$T = \frac{1}{2}\rho_0 \int d\boldsymbol{r} |\delta \dot{\boldsymbol{s}}(\boldsymbol{r}, t)|^2 \equiv \frac{1}{2}\sum_n B_n |\dot{\alpha}_n|^2. \quad (18)$$

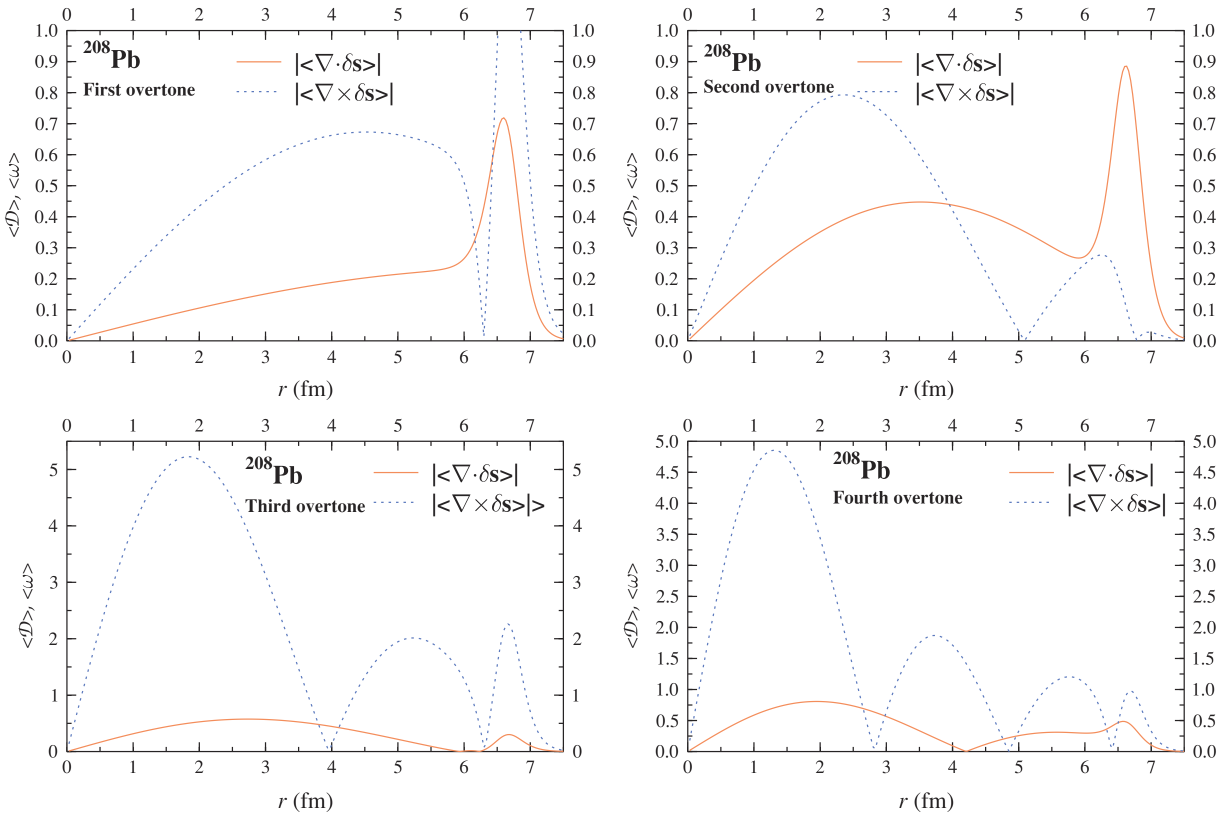

FIG. 2. (Color online) Compressibility and vorticity of the first four overtones of the ISGDR in ^{208}Pb.

For the mass inertia parameter, we derive the expression

$$B_n = \frac{3mA}{4\pi}\left\{\left[\frac{1}{2}\left(j_0^2(k_L^{(n)}R_0) + j_1^2(k_L^{(n)}R_0)\right) - \frac{1}{2k_L^{(n)}R_0} \times j_1(k_L^{(n)}R_0)\left(j_0(k_L^{(n)}R_0) + \frac{6}{k_L^{(n)}R_0}j_1(k_L^{(n)}R_0)\right)\right] + r_n^2\left[\frac{1}{2}\left(j_0^2(k_T^{(n)}R_0) + j_1^2(k_T^{(n)}R_0)\right) - \frac{1}{2k_T^{(n)}R_0} \times j_1(k_T^{(n)}R_0)\left(j_0(k_T^{(n)}R_0) + \frac{6}{k_T^{(n)}R_0}j_1(k_T^{(n)}R_0)\right)\right]\right\}. \tag{19}$$

The stiffness coefficient associated with an oscillation of degree n is simply

$$C_n = \Omega_n^2 B_n,$$

and the quantized form of the energy can be obtained by introducing the creation and annihilation dipole "gions" [34]

$$\hat{d}_n^+ = \left(\frac{\Omega_n B_n}{2\hbar}\right)^{\frac{1}{2}}\left(\alpha_n - \frac{i}{\Omega_n}\dot{\alpha}_n\right),$$

$$\hat{d}_n = \left(\frac{\Omega_n B_n}{2\hbar}\right)^{\frac{1}{2}}\left(\alpha_n + \frac{i}{\Omega_n}\dot{\alpha}_n\right).$$

The collective Hamiltonian will then read

$$\hat{H} = \sum_n \hbar\Omega_n\left(\hat{d}_n^\dagger\hat{d}_n + \frac{1}{2}\right). \tag{20}$$

The mass parameter can also be used as a measure of vorticity in nuclear fluid dynamics. To assess the change in this quantity due to the vorticity, a comparison with the mass parameter from the purely compressional variant of the ISGDR, as the one derived by Kolomietz and Shlomo in [16], is required. However, one must not overlook that when one discards the transverse field (12), the boundary conditions (16) provide different roots of k_L. The first overtone of compressional mode is $\hbar\Omega_1 = 22.3$ MeV ($3.23\hbar\omega_0$) for ^{208}Pb, a value very close not only to the one derived in [16] as expected, but also to the second overtone listed in Table I when vortical admixtures are present (the mode around $3\hbar\omega$). Because the first overtone from Table I is not present in the case when the displacement field is limited to its irrotational component, we are then left to compare the mass parameter of the first overtone obtained in the irrotational case with the second mode obtained in the mixed case. For the high-lying ISGDR ($3\hbar\omega$ mode) of ^{208}Pb, the mass parameter (19), when the velocity field is supplemented with the transverse component, increases by about 75% compared to the irrotational value.

Before ending this section, one should address an issue related to the approximations that lead to the above predictions. From the point of view of the nuclear Fermi-fluid model, the truncation that leads to the set of equations of motion (7) corresponds to the restriction of the highest multipolarity $l_{\max} = 2$ of the Fermi surface distortion (see, for example, [39]). If the number of multipoles in the Fermi surface distortion is increased, a significant variation takes place, specially for the transverse sound speed. If one considers the next truncation ($l_{\max} = 3$) and one keeps fixed the Fermi parameters used in the computation of the elastic Lamé constants for the truncation $l_{\max} = 2$, then one finds that the lowest root of the longitudinal sound mode c_L is varying only by a few percent. The transverse sound mode c_T displays instead a considerable variation. However, to assess the putative dramatic change in the overtones, there are also other constraints and parameters of the model that have to be reconsidered. If one adopts a poor approximation and use inside the boundary conditions for a free surface for $l_{\max} = 2$, the values of c_L and c_T for truncation $l_{\max} = 3$, one obtains that the first overtone of the ISGDR lays close to the experimental high-energy mode and thus the low-energy mode, previously found for $l_{\max} = 2$ disappears. The boundary conditions for $l_{\max} = 3$ must change since the analog of the stress tensor in this case will include also velocity-dependent terms. If we consider the same type of free surface, we have to augment the boundary conditions also with constraints for the velocity field on the surface. Obviously, one would then also get different values for k_L and k_T. However, as advocated until recently [16,40], it seems that the limitation to monopole, dipole, and quadrupole distortions of the Fermi surface in the study of giant resonances is a satisfactory approximation. The satisfactory agreement with data obtained in inelastic α scattering reported in this paper seems to strengthen this conclusion. This does not mean that the extension to higher multipole distortions of the Fermi surface should not be explored in the near future in order to address unanswered questions regarding the ISGDR.

III. ELECTROMAGNETIC STRUCTURE OF ISGDR

A. Low-*q* limit of the form-factor multipole parametrization

To disclose the structure of the ISGDR, we adopt the multipolar parametrization of charges and currents according to [19]. In this approach, the classical electromagnetic multipoles are expanded in the momentum transfer in reactions with photons, electrons, or charged hadrons. Let us first take the charge multipole form factor for the charge part of the ISGDR fluctuation density:

$$M^{C}_{\lambda\mu}(q,t) = \int d\boldsymbol{r}\, j_\lambda(qr) Y_{\lambda\mu}(\vartheta\varphi)\delta\rho_p(\boldsymbol{r},t) \approx \frac{q^\lambda}{(2\lambda+1)}\left(Q_{\lambda\mu}(t) - \frac{1}{2(2\lambda+3)}q^2\overline{\varrho^2_{\lambda\mu}}(t)\right). \quad (21)$$

The first term of the above q expansion represent the transition charge dipole moment

$$Q_{\lambda\mu}(t) = \delta_{\lambda,1}\delta_{\mu,0}\int d\boldsymbol{r} r^\lambda Y_{\lambda\mu}(\theta,\phi)\delta\rho_p(\boldsymbol{r},t) = 0, \quad (22)$$

a quantity which vanishes for the ISGDR because of the constraint imposed on the c.m. motion. For the IVGDR this will not be the case, since the dynamic dipole moment arises naturally as a measure of the relative motion between the negative charge (neutron) distribution and the positive charge (proton) distribution. Instead, the next term in the expansion (21) does not cancel. The quantity

$$\overline{\varrho^2_{\lambda\mu}}(t) = \delta_{\lambda,1}\delta_{\mu,0}\int d\boldsymbol{r} r^{\lambda+2} Y_{\lambda\mu}(\theta,\phi)\delta\rho_p(\boldsymbol{r},t) = 2\rho_{0p}R_0^5\delta_{\lambda,1}\delta_{\mu,0}\sum_n \alpha_n(t)\frac{j_\lambda\left(k_L^{(n)}R_0\right)}{k_L^{(n)}R_0} \quad (23)$$

represents the mean square radius of the dipole charge distribution. It provides information on the spatial extension of the ISGDR, and it depends only on the longitudinal (compressional) part of the displacement field which is related via the continuity equation (2) to the density fluctuations.

According to the charge-current multipole parametrization of [19], the electric transverse form factor splits into the $q = 0$ limit and a term containing the higher-order content in q.

$$T^E_{\lambda\mu}(q,t) = \frac{i^{\lambda+1}}{(2\lambda+1)!!}q^{\lambda-1}\sqrt{\frac{\lambda+1}{\lambda}}\left(\dot{Q}_{\lambda\mu}(0,t) + q^2 T^{\text{tor}}_{\lambda\mu}(q,t)\right). \quad (24)$$

The first term within the large parentheses is the time derivative of the Coulomb multipole moment defined in Eq. (22); the second term represents the toroidal form factor that reads in the low-q limit as

$$T^{\text{tor}}_{\lambda\mu}(0,t) = \frac{1}{2i}\sqrt{\frac{\lambda}{\lambda+1}}\frac{1}{2\lambda+3}\int d\boldsymbol{r}\, r^{\lambda+2}\boldsymbol{Y}^\mu_{\lambda\lambda}\cdot(\nabla\times\boldsymbol{j}(\boldsymbol{r},t)). \quad (25)$$

In classical electrodynamics, the transition toroidal multipole moment is associated with a poloidal flow on the wings of a toroidal solenoid (for details, see the reviews [19]). In the study of electric collective states, it can be related to the strength of the vorticity associated with a nuclear transition. Indeed, following Ref. [41], we introduce the transition multipoles of the curl of the current density (unconstrained by the charge-current conservation law),

$$\mathcal{T}_{\lambda\lambda}(r) \equiv \langle I_f\|(\nabla\times\boldsymbol{j}(\boldsymbol{r},t))_{\lambda\lambda}\|I_i\rangle.$$

In order to remove the charge-current conservation constraint, the authors of [41] introduced the pure vorticity transition multipole

$$\omega_{\lambda\lambda} = \mathcal{T}_{\lambda\lambda'}(r) - \sqrt{\frac{\lambda+1}{\lambda}}\Omega\rho_\lambda, \quad (26)$$

where ρ_λ is the charge density multipole and Ω the frequency of the quanta associated with the transition. Defining the quantity

$$\nu_\lambda = \int_0^\infty dr\, r^{\lambda+4}\omega_{\lambda\lambda}(r)$$

according to [41] as the strength of the vorticity and employing the definitions (23) for the square of the dynamic dipole charge distribution and (25) for the dynamic dipole toroidal moment, we arrive at the expression relating the reduced matrix elements (r.m.e.) of these last two electromagnetic multipoles

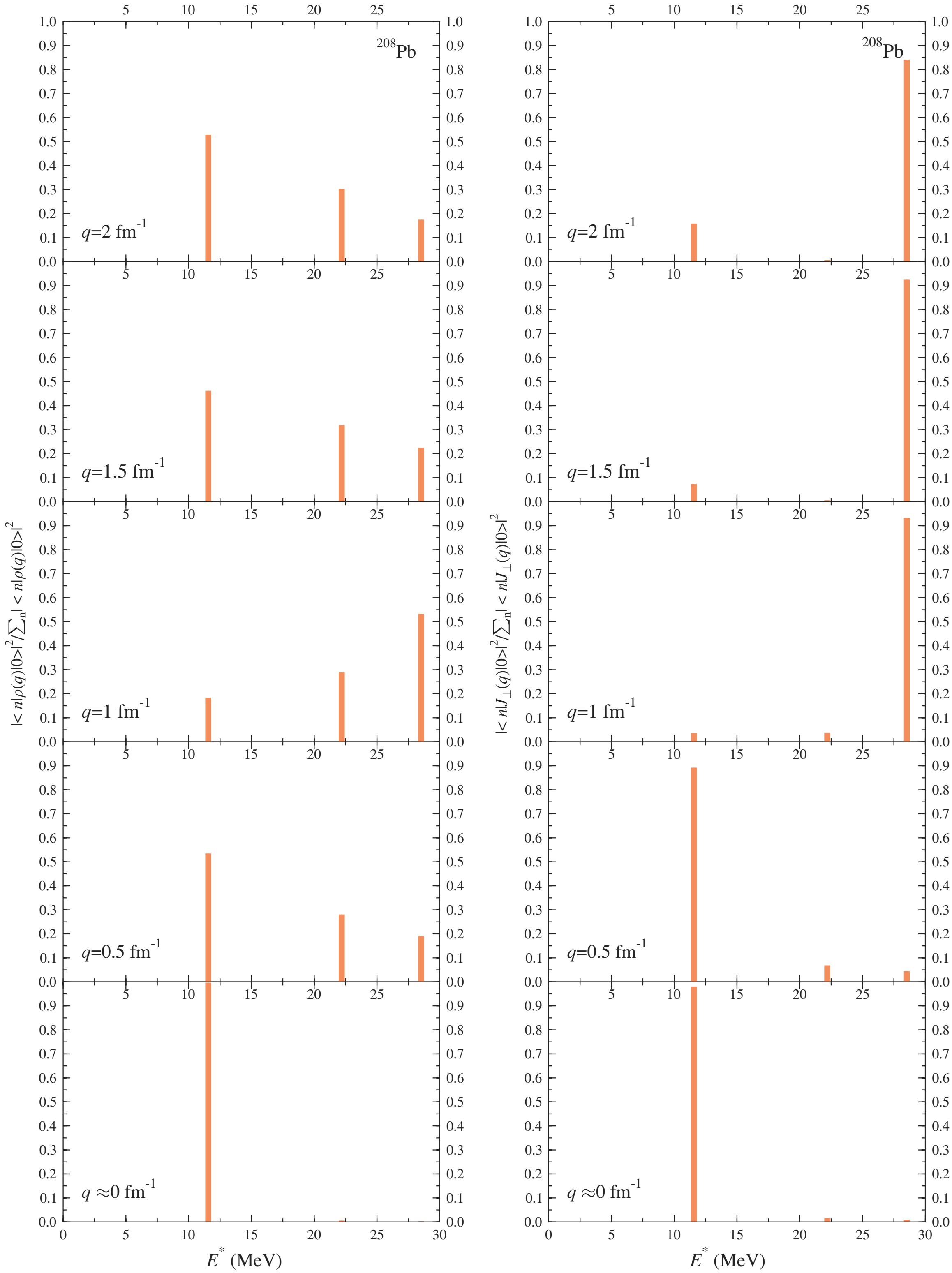

FIG. 3. (Color online) Zero-order energy strengths distributions for ρ and $\boldsymbol{J}_\perp$. Energy cut $(E^*)_{\rm cut} = 30$ MeV.

and the vorticity strength

$$\langle I_f = 1_n^- \| T_1^{\rm tor} \| I_i = 0\rangle = \frac{i}{10}\left[\frac{1}{\sqrt{2}}\nu_1 + \Omega_n \langle I_f = 1_n^- \| \overline{\varrho_1^2} \| I_i = 0\rangle\right]. \tag{27}$$

From this last formula, we see that since the toroidal dipole moment and the square radius of the dipole charge distribution are the leading terms in the q expansion of the transverse electric (24) and Coulomb (21) form factors for the ISGDR, the determination of these two electromagnetic multipoles

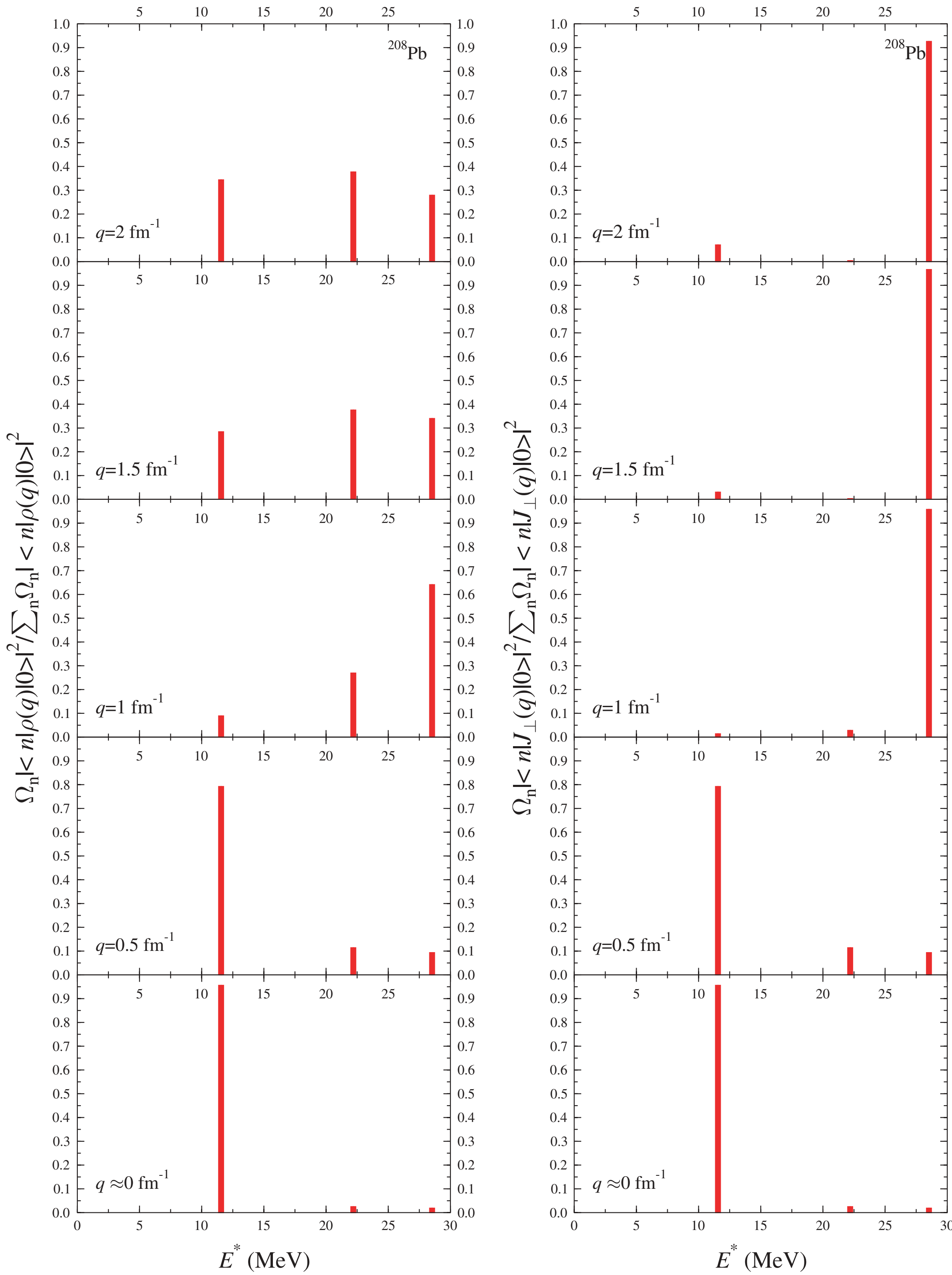

FIG. 4. (Color online) First-order energy strengths distributions for ρ and $\boldsymbol{J}_\perp$. Energy cut $(E^*)_{\rm cut} = 30$ MeV.

at low q allows the determination of the vorticity content unconstrained by the charge-current conservation law. Before ending this section, we give the classical expression of the transition toroidal dipole moment associated with the ISGDR. Since the current density reads in this case

$$\boldsymbol{j} = e\frac{Z}{A}n_0\sum_{n=1}\left(\delta \boldsymbol{s}_L^{(n)}(\boldsymbol{r}) + r_n\delta \boldsymbol{s}_T^{(n)}(\boldsymbol{r})\right), \tag{28}$$

we finally obtain

$$T_1^{\rm tor}(0,t) = \frac{1}{10\sqrt{2}}\rho_{0p}R_0^5\sum_n r_n\dot{\alpha}_n(t)\frac{j_3\big(k_T^{(n)}R_0\big)}{k_T^{(n)}R_0}. \quad (29)$$

Thus, the dipole toroidal moment depends only on the shear (vortical) part of the proton fluid displacement field.

B. Sum rules for electroexcitation

Inelastic electron scattering is an excellent tool for exploring the nature of currents involved in the excitation of low-lying (rotational or vibrational) and high-lying (giant resonances) collective states [42]. A specific feature of this reaction is represented by the possibility of separating the longitudinal from the transverse response functions. This is of vital importance if one tries to disentangle the compressional from the vortical response in the excitation of a specific electric collective state.

It is known that for the isoscalar electric modes simulated by operators depending only on coordinates of the particles, the energy-weighted sum rules can be determined model independently, and they depend only on the ground-state properties of the nucleus [5,6,36,43]. Operators from this class are commuting with interactions that do not depend explicitly on the momenta of the particles. These scalar operators are simulating shape or density distortions corresponding to a given isoscalar multipolar resonance; for that reason, in the literature the macroscopic images associated with these excitations are always irrotational surface or bulk compressional oscillations. They are inadequate for describing distortions of the nuclear current which are not constrained by the charge-current conservation law, i.e., excitations with vortical currents. A class of sum rules coping with both kind of distortions, i.e., of charge density and current (unconstrained by the charge-current relations), is given by the longitudinal L and transverse T intrinsic energy-weighted sum rules (EWSR) at constant three-momentum transfer $|\boldsymbol{q}|$; the EWSR are constructed by weighting the nuclear response functions [44]

$$R^L(\boldsymbol{q},E^*) = \sum_n^\infty |\langle n|\rho(\boldsymbol{q})|0\rangle|^2\delta\left(E^* - \frac{\hbar^2q^2}{2M_A} - E_n\right), \quad (30)$$

$$R^T(\boldsymbol{q},E^*) = \sum_n^\infty |\langle n|\boldsymbol{J}_\perp(\boldsymbol{q})|0\rangle|^2\delta\left(E^* - \frac{\hbar^2q^2}{2M_A} - E_n\right), \quad (31)$$

with an appropriate power of the nuclear excitation energy E^*. Summing over all excited states, we obtain the intrinsic p-order EWSR depending on q

$$m_p^L(q) = \int dE^{*\prime}R^L(\boldsymbol{q},E^{*\prime})E^{*p} = \sum_n^\infty E_n^p\langle n|\rho(\boldsymbol{q})|0\rangle|^2, \quad (32)$$

$$m_p^T(q) = \int dE^{*\prime}R^T(\boldsymbol{q},E^{*\prime})E^{*\prime p} = \sum_n^\infty E_n^p\langle n|\boldsymbol{J}_\perp(\boldsymbol{q})|0\rangle|^2, \quad (33)$$

where $E^{*\prime} = E^* - \hbar^2q^2/2M_A$ is the energy available for intrinsic excitations, and $\boldsymbol{J}_\perp(\boldsymbol{q})$ denotes the transverse component of the current operator relative to the momentum transfer $(\boldsymbol{J}_\perp(\boldsymbol{q}) = \boldsymbol{J}(\boldsymbol{q}) - \boldsymbol{q}(\boldsymbol{q}\cdot\boldsymbol{J})/\boldsymbol{q}^2)$.

The longitudinal and transverse p-order energy strengths of each state can then be obtained as relative contributions to the corresponding sum rules (32) and (33)

$$E_n^p|\langle n|\rho(\boldsymbol{q})|0\rangle|^2/m_p{}^L(q),$$
$$E_n^p|\langle n|\boldsymbol{J}_\perp(\boldsymbol{q})|0\rangle|^2/m_p{}^T(q).$$

In Figs. 3 and 4, we represent the zero- and first-order strength distributions for the longitudinal and transverse responses. In the sums, only the first three overtones were included and therefore the excitation energy is truncated at 30 MeV. We see that for very low momentum transfer, the L and T strengths are mainly concentrated on the first overtone. When q increases, the L and T strengths follow a different pattern. While the L strength is fragmented almost equally over the three overtones, the T strength is undergoing a transition from a low-q regime where the first overtone dominates to a high-q regime where the third overtone becomes predominant. For both regimes, the second overtone plays a very minor role. This fact can be explained in our view by the compressibility content of this mode which is "washed out" in the transverse response function. In the longitudinal response, the second overtone plays a more visible role.

In the low-q limit, the ratios m_1/m_0 and $\sqrt{m_3/m_1}$ are expected to provide crude estimates of the mean excitation energies associated with the density or transverse density current distortions. Table II lists these mean excitation energies for a series of spherical nuclei. Comparing the obtained values to the eigenvalues of the first two overtones and the most recent experimental data from Refs. [2] and [3], we notice that the high-energy component is for all the studied nuclei

TABLE II. Ratios of ISGDR sum rules for $q \longrightarrow 0$ compared to the energies of the first two overtones for ^{90}Zr, ^{116}Sn, ^{144}Sm, and ^{208}Pb and with the latest experimental data from Refs. [2] and [3] for the low- and high-energy peaks.

Nucleus	$m_1{}^L/m_0{}^L$ (MeV)	$\sqrt{m_3{}^L/m_1{}^L}$ (MeV)	$m_1{}^T/m_0{}^T$ (MeV)	$\sqrt{m_3{}^T/m_1{}^T}$ (MeV)	$\hbar\Omega_1$ (MeV)	$\hbar\Omega_2$ (MeV)	$(\hbar\Omega_1)_{\rm exp}$ (MeV)	$(\hbar\Omega_2)_{\rm exp}$ (MeV)
^{90}Zr	15.44	16.29	16.86	25.53	15.28	29.34	16.20 ± 0.80	25.70 ± 0.70 [2]
^{116}Sn	14.19	14.99	15.51	23.68	14.04	26.96	14.38 ± 0.25	25.50 ± 0.60 [2]
							14.70 ± 0.80	23.00 ± 0.60 [3]
^{144}Sm	13.21	14.07	14.64	23.95	13.07	25.08	14.00 ± 0.30	24.51 ± 0.40 [2]
^{208}Pb	11.68	12.44	12.96	21.19	11.56	22.19	13.26 ± 0.30	22.20 ± 0.30 [2]
							12.50 ± 0.30	22.50 ± 0.30 [3]

satisfactorily reproduced by $\sqrt{m_3{}^T/m_1{}^T}$, whereas the ratio of longitudinal sum rules $m_1{}^L/m_0{}^L$ provides a rather coarse approximation of the low-energy resonance. Better estimates of the first overtone are given by $\sqrt{m_3{}^L/m_1{}^L}$ and $m_1{}^T/m_0{}^T$, depending also on which experimental set of data one is willing to give preference. The fact that the two lowest peaks can be reproduced by either a longitudinal or a transverse ratio of sum rules should not be surprising. As we saw in the previous section, the two components of the resonance have a mixed longitudinal-transverse content.

IV. SUMMARY AND CONCLUSIONS

The lower and upper component of the ISGDR, as reported by the latest experimental measurements, are explained as the first two overtones of a spherical Fermi-fluid system with a sharp free surface corresponding to a mixture of dipole compression and vorticity oscillations.

The approach presented in this work was applied primarily to the heavy spherical nucleus ^{208}Pb, because in this case the sharp-edge density distribution assumption is more acceptable as would be the case for lighter nuclei for which experimental data on ISGDR are available (^{40}Ca, ^{90}Zr, ^{116}Sn, and ^{144}Sm) and where the diffuse surface plays an important role. In order to extend the analysis of ISGDR to these nuclei and to exotic nuclei that are presently under intense investigation, one should first adopt a more realistic assumption for the ground-state density distribution. In this case along with the density, other parameters of the nuclear Fermi liquid, e.g., the Lamé coefficients, acquire a radial dependence, and the equations of motion must be solved numerically.

In the present approach, the excitation of the ISGDR is not limited to the squeezing operator. It includes the entire momentum content in the operator $j_1(kr)Y_1(\hat{r})$ and takes into account also its c.m. correction via constraints on the density and displacement field fluctuations. Moreover, since there is no mathematical or physical exception, it considers along with the longitudinal solution, the transverse solution of the vector Helmholtz equation. Consequently, the overtones of the ISGDR are mixtures of compressional and vortical velocity fields. For the second overtone, previously advocated to be of compressional nature, the nuclear Fermi-fluid approach confirms very recent microscopic predictions [25] that point toward a coexistence of compressional and vorticity vibrations in the ISGDR states up to 30 MeV. It should also be mentioned that the energy of the second overtone is close to the energy of the first overtone extracted in the case when the transverse part of the displacement field is disregarded. Thus, the inclusion of vortical components in the evaluation of the energy centroids gives rise to the low-lying component (first) overtone of the ISGDR.

Naturally, a question arises: Has there been any experimental indication of the overtones with $n \geqslant 3$, located above the high-lying ISGDR state? For now, this question cannot be answered because the latest data reported by the College Station group [2] show very large uncertainties in the strength distribution for ^{208}Pb beyond the second peak, i.e., at excitation energy $>3\hbar\omega$.

A study undertaken of the electromagnetic multipole transitions concluded that the leading term in the Coulomb form factor is singled out only by the density fluctuation and can be related to the rms-charge radii. In turn, the leading multipole in the transverse electric form factor, the toroidal dipole moment, results solely from the transverse part of the velocity field. In this respect the r.m.e. of the toroidal dipole transition provides a signature of vorticity through electromagnetic probes.

The (e, e') are promising candidates for the exploration of the role of longitudinal and vortical currents of ISGDR since the separation of longitudinal (Coulomb) and electric transverse form factors is feasible. However, in such reactions it is difficult to avoid the excitation of the dominant electric dipole response, the IVGDR. It would be in this respect interesting to search for a macroscopic description that deals in a unified manner with the isoscalar and isovector electric dipole responses.

ACKNOWLEDGMENTS

The author aknowledges with gratitude the financial support from the Alexander von Humboldt Foundation and the warm hospitality of Prof. A. Richter at the Institut für Kernphysik, TU-Darmstadt, where this work was performed. He also acknowledges useful discussions with Prof. P. v. Neumann-Cosel and Dr. V. I. Ponomarev.

APPENDIX: SCALAR AND VECTOR HELMHOLTZ EQUATIONS

The solution of the scalar Helmholtz equation (HE) (9) reads

$$\mathcal{D} = \sum_{\lambda\mu} a_{\lambda\mu} j_\lambda(k_L r) Y_{\lambda\mu}(\theta, \phi). \tag{A1}$$

The solution of the vector HE splits into an electric (poloidal) and a magnetic (torsional) solution

$$\boldsymbol{\omega}^{\text{pol}} = \sum_{\lambda\mu} b^{\text{el}}_{\lambda\mu} j_\lambda(k_T r) \boldsymbol{Y}^{\mu}_{\lambda\lambda}(\theta, \phi) \tag{A2}$$

$$\begin{aligned}\boldsymbol{\omega}^{\text{tor}} = \sum_{\lambda\mu} b^{\text{el}}_{\lambda\mu} \frac{1}{\sqrt{2\lambda+1}} (\delta_{\lambda'\lambda-1}\sqrt{\lambda+1} - \delta_{\lambda'\lambda+1}\sqrt{\lambda}) \\ \times j_{\lambda'}(k_T r) \boldsymbol{Y}^{\mu}_{\lambda\lambda'}(\theta, \phi).\end{aligned} \tag{A3}$$

In the present study on electric resonances, we are interested only in the poloidal solution. Using the properties of the spherical harmonic vectors, we can derive the expression of the longitudinal and transverse displacement fields. Since $\delta \boldsymbol{s}_L$

results from the definition of the scalar function

$$\mathcal{D} \equiv \nabla \cdot \delta \boldsymbol{s} = \nabla \cdot \delta \boldsymbol{s}_L, \tag{A4}$$

we have that

$$\delta \boldsymbol{s}_L = -\frac{1}{k_L} \sum_{\lambda\mu} a_{\lambda\mu} \frac{1}{\sqrt{2\lambda+1}} (\delta_{\lambda'\lambda-1}\sqrt{\lambda'+1} + \delta_{\lambda'\lambda+1}\sqrt{\lambda'}) \times j_{\lambda'}(k_L r) \boldsymbol{Y}^{\mu}_{\lambda\lambda'}(\theta,\phi). \tag{A5}$$

Similarly, from the definition of the vorticity

$$\boldsymbol{\omega}^{\rm pol} \equiv \tfrac{1}{2}\nabla \times \delta \boldsymbol{s}_T, \tag{A6}$$

we get

$$\delta \boldsymbol{s}_T = \frac{i}{k_T} \sum_{\lambda\mu} b_{\lambda\mu} \frac{1}{\sqrt{2\lambda+1}} (\delta_{\lambda'\lambda+1}\sqrt{\lambda'} - \delta_{\lambda'\lambda+1}\sqrt{\lambda'-1}) \times j_{\lambda'}(k_T r) \boldsymbol{Y}^{\mu}_{\lambda\lambda'}(\theta,\phi). \tag{A7}$$

[1] H. L. Clark, Y.-W. Lui, and D. H. Youngblood, Phys. Rev. C **63**, 031301(R) (2001).
[2] D. H. Youngblood, Y.-W. Lui, B. John, Y. Tokimoto, H. L. Clark, and X. Chen, Phys. Rev. C **69**, 054312 (2004).
[3] M. Uchida *et al.*, Phys. Lett. **B557**, 12 (2003).
[4] H. P. Morsch, P. Decowski, M. Rogge, P. Turek, L. Zemlo, S. A. Martin, G. P. A. Berg, W. Hurlimann, J. Meissburger, and J. G. M. Romer, Phys. Rev. C **28**, 1947 (1983).
[5] J. J. Deal, Nucl. Phys. **A217**, 210 (1973).
[6] M. N. Harakeh and A. E. L. Dieperink, Phys. Rev. C **23**, 2329 (1981).
[7] J. Wambach, V. Klemt, and J. Speth, Phys. Lett. **B77**, 245 (1978).
[8] N. Van Giai and H. Sagawa, Nucl. Phys. **A371**, 1 (1981).
[9] I. Hamamoto, H. Sagawa, and X. Z. Zhang, Phys. Rev. C **57**, R1064 (1998).
[10] T. S. Dumitrescu and F. E. Serr, Phys. Rev. C **27**, 811 (1983).
[11] G. Coló, N. Van Giai, P. F. Bortignon, and M. R. Quaglia, Phys. Lett. **B485**, 362 (2000).
[12] S. Shlomo and A. I. Sanzhur, Phys. Rev. C **65**, 044310 (2002).
[13] M. L. Gorelik, I. V. Safonov, and M. H. Urin, Phys. Rev. C **69**, 054322 (2004).
[14] D. Vretenar, A. Wandelt, and P. Ring, Phys. Lett. **B487**, 334 (2000).
[15] K. Woeste, Z. Phys. **133**, 370 (1952).
[16] V. M. Kolomietz and S. Shlomo, Phys. Rev. C **61**, 064302 (2000); Phys. Rep. **390**, 133 (2004).
[17] G. Holzwarth and G. Eckardt, Nucl. Phys. **A325**, 1 (1979).
[18] S. F. Semenko, Yad. Fiz. **34**, 639 (1981) [Sov. J. Nucl. Phys. **34**, 356 (1981)].
[19] V. M. Dubovik and A. A. Cheshkov, Fiz. Elem. Chastits At. Yadra **5**, 792 (1974) [Sov. J. Part. Nucl. **5**, 318 (1975)]; V. M. Dubovik and V. V. Tugushev, Phys. Rep. **187**, 145 (1990).
[20] E. B. Balbutsev and I. N. Mikhailov, J. Phys. G **14**, 545 (1988).
[21] S. I. Bastrukov, Ş. Mişicu, and V. I. Sushkov, Nucl. Phys. **A562**, 191 (1993).
[22] Ş. Mişicu, Dissertation, Institute for Atomic Physics, 1995 (in Romanian) [abridged English version, Rom. J. Phys. **43**, 193 (1998)].
[23] Ş. Mişicu, J. Phys. G: Nucl. Part. Phys. **21**, 669 (1995).
[24] I. N. Mikhailov, Ch. Briançon, and P. Quentin, Fiz. Elem. Chastits At. Yadra **27**, 303 (1996).
[25] D. Vretenar, N. Paar, P. Ring, and T. Nikšić, Phys. Rev. C **65**, 021301(R) (2002).
[26] Ş. Mişicu and S. I. Bastrukov, Eur. Phys. J. A **13**, 399 (2002).
[27] N. Ryezayeva, T. Hartmann, Y. Kalmykov, H. Lenske, P. vonNeumann-Cosel, V. Y. Ponomarev, A. Richter, A. Shevchenko, S. Volz, and J. Wambach, Phys. Rev. Lett. **89**, 272502 (2002).
[28] C.-Y. Wong and N. Azziz, Phys. Rev. C **24**, 2290 (1981).
[29] Arnold Sommerfeld, *Mechanik der deformierbaren Medien* (Verlag Harri Deutsch, Frankfurt am Main, 1978) [English transl., *Mechanics of Deformable Bodies* (Academic, New York, 1950)].
[30] J. P. Blaizot, Phys. Rep. **64**, 171 (1980).
[31] Ari Ben-Menahem and Sarva Jit Singh, *Seismic Waves and Sources* (Springer-Verlag, New York, 1981).
[32] P. M. Morse and H. Feschbach, *Methods of Theoretical Physics* (McGraw-Hill, New York, 1953), Parts 1 and 2.
[33] S. I. Bastrukov, J. Libert, and I. V. Molotsova, Int. J. Mod. Phys. E **6**, 89 (1997).
[34] J. Eisenberg and W. Greiner, *Nuclear Models* (North-Holland, Amsterdam, 1970), Vol. 1.
[35] G. Eckart, G. Holzwarth, and J. P. da Providencia, Nucl. Phys. **A364**, 1 (1981).
[36] A. Bohr and B. R. Mottelson, *Nuclear Structure* (Benjamin, Amsterdam, 1974), Vol. 2.
[37] F. E. Serr, T. S. Dumitrescu, T. Suzuki, and C. H. Dasso, Nucl. Phys. **A404**, 359 (1983); T. S. Dumitrescu, C. H. Dasso, F. E. Serr, and T. Suzuki, J. Phys. G **12**, 349 (1986).
[38] E. Feenberg, *Theory of Quantum Fluids* (Academic, New York, 1969).
[39] T. Yukawa and G. Holzwarth, Nucl. Phys. **A364**, 29 (1981).
[40] S. Shlomo and V. M. Kolomietz, Rep. Prog. Phys. **68**, 1 (2005).
[41] D. G. Ravenhall and J. Wambach, Nucl. Phys. **A475**, 468 (1987).
[42] H. Überall, *Electron Scattering from Complex Nuclei,* (Academic, New York, 1971), Part A.
[43] E. Lipparini and S. Stringari, Phys. Rep. **175**, 103 (1989).
[44] V. Tornow *et al.*, Nucl. Phys. **A348**, 157 (1980).